Nanotechnology Perceptions
ISSN 1660-6795
www.nano-ntp.com

Optimization of Shell and Tube Heat Exchangers through Numerical Study

Hemavathi P, Vijaya Kumar Reddy K

Department of Mechanical Engineering, JNTUH College of Engineering, Hyderabad
Email: hhemapattu8@gmail.com

Shell and tube heat exchangers are widely used in industries due to their ease of cleaning and adaptability, essential for efficient heat management. This study numerically examines heat transfer efficiency with 22% cut segmental baffles and helical baffles (200, 300, 400, and 500). Results show that 22% cut segmental baffles achieve a higher heat transfer coefficient compared to continuous helical baffles. Heat transfer efficiency increases with mass flow rate for all configurations: improvements of 34.75%, 58.87%, 71.70%, and 80.08% for 200, 300, 400, and 500 helical baffles, respectively, were observed relative to the 22% cut segmental baffle. However, as the helix angle of baffles increases, the heat transfer coefficient decreases, with deviations of 26.89%, 28.94%, 50.87%, 63.57%, and 72.49% observed in comparison to the 22% cut segmental baffle at the same water flow rate.
Keywords: heat exchangers, baffles.

1. Introduction

Shell and tube heat exchangers are widely used in various industries, including chemical, food, power engineering, refrigeration, and air conditioning. They play a critical role in applications such as boilers, oil coolers, condensers, and pre-heaters due to their robustness and ability to handle high-pressure operations.

The study of their design, thermal analysis, and construction is essential for mechanical, thermal, and chemical engineering scholars, as it is a fundamental aspect of their curriculum and research. Understanding the basic configuration and performance of shell and tube heat exchangers is crucial for practicing engineers, given their extensive use throughout the process industry.

2. Literature Review:

Roetzel & Lee (1993) [2]Variables: Stream flow direction, shell side flow rate, tube side flow rate, clearance, and distance between baffles.Findings: Peclet number depends only on geometry, not on Reynolds number.

Waseem Al Hadad et al. (2019) [3]Method: Proposed an impulse response technique for fouling detection.Conclusion: Impulse response can effectively detect fouling in heat exchangers.

Huadong Li & Volker Kottke (1998) [4]Focus: Pressure drop and heat transfer response due to baffle-shell leakage.Results: Pressure drop coefficient reduced by up to 74% at Re=500 and 69% at Re=16,000 due to shell side leakages.

Wilfried Reotzel & Deiying W Lee (1994) [5]Study: Influence of baffle/shell leakage on thermal performance.Outcome: Peclet number is geometrically dependent; baffle-shell clearance impacts can be expressed empirically.

Halle H et al. (1988) [6]Experiment: Pressure drop for various segmentally baffled configurations.Findings: Overall pressure drop varied significantly with nozzle size and tube layout.

Mustapha Mellal et al. (2017) [8]Study: Turbulent flow and heat transfer with varying baffle spacing and orientation angles.Results: 180° orientation at 64 mm spacing had the highest heat transfer coefficient.

Anuruddha Bhattacharjee et al. (2017) [9]Research: Baffle configurations with different helix angles.Conclusion: 25.52° helix angle was most effective; 10.81° performed poorly.

Asif Ahmed et al. (2017) [10]Comparison: Segmental vs. helical baffles.Results: Helical baffles showed 72-127% higher heat transfer coefficient with 59-63% lower pressure drop.

Bashir I Master et al. (2003) [11]Findings: Helixchanger heat exchangers showed 50% higher duty and extended run lengths between cleaning.

Cong Dong et al. (2014) [13]Study: Flow and heat transfer characteristics of tri-sectional helical baffles.Conclusion: Circumferential overlap scheme yielded highest heat transfer coefficients.

Jian Chen et al. (2020) [17]Research: Unilateral ladder type helical baffle vs. segmental baffle.Results: 15.3-47.1% reduction in pressure drop with improved heat transfer coefficients.

Ya Ping Chen et al. (2013) [36]Focus: Trisection helical baffle heat exchangers.Conclusion: Secondary flows enhanced heat transfer and reduced fouling.

Yong Gang Lei et al. (2008) [38]Study: Impact of baffle inclination angles.Results: Increased Nusselt number with angle up to 30°, decreased pressure drop compared to segmental baffles.

- Helical Baffles: Generally outperform segmental baffles in heat transfer efficiency and pressure drop.

- Design Variables: Helix angle, baffle spacing, and configuration significantly affect performance metrics such as heat transfer coefficient and pressure drop.
- Fouling and Leakage: Effective detection methods and understanding of leakage effects are crucial for optimizing heat exchanger performance.

Data reduction

The tube pitch is $P_t=1.25d_0$ (1)

Where Pt is the tube pitch in mm

d_0 is the outer diameter of the tube in mm

Tube pitch ratio $P_r = \frac{P_t}{d_0}$ (2)

Inside diameter of tube $d_i=0.8d_0$ (3)

Where di is the inner diameter of the tube in mm

Diameter ratio $d_r = \frac{d_0}{d_i}$ (4)

Tube clearance $C_t = P_t - d_0$ (5)

The equivalent/hydraulic diameter for square patterns

$$D_e = \frac{4\left(P_t^2 - \left(\frac{\pi d_0^2}{4}\right)\right)}{\pi d_0} \quad (6)$$

Equivalent diameter varies with the flow arrangements.

For square tube pitch

$$D_e = \frac{1.27}{d_0}(P_t^2 - 0.785d_0^2) \quad (7)$$

For triangular tube pitch

$$D_e = \frac{1.10}{d_0}(P_t^2 - 0.917d_0^2)$$

The constant values of K1 and n1 for different tube configurations are given in Table 1. These values are coefficients that are taking values according to flow arrangements and number of passes. For different arrangements these coefficients are shown in this below table.

Table 1: Values of constants

No. of passes	Triangular Pitch		Square and Rotated Square Pitch	
	K_1	N_1	K_1	n_1
1	0.319	2.142	0.215	2.207

2	0.249	2.207	0.156	2.291
4	0.175	2.285	0.158	2.263
6	0.0743	2.499	0.0402	2.617
8	0.0365	2.675	0.0331	2.643

Number of tubes is calculated by $N_t = K_1 \left(\frac{D_g - 0.02}{d_0}\right)^{n_1}$ (8)

$$N_t = K_1 \left(\frac{D_s}{d_0}\right)^{n_1} \quad (9)$$

Number of tubes given as

Where N_t is number of tubes,

Author going to consider 4 number of tubes. (only integer values are considering)

$$D_{\text{otl}} = d_0 \left(\frac{N_t}{K_1}\right)^{\frac{1}{n_1}} \quad (10)$$

Tube bundle outer diameter

The shell diameter is $D_s = \frac{D_{\text{otl}}}{0.95} + \delta_{\text{sb}}$ (11)

Where $\delta_{\text{sb}}$is shell to baffle clearance,

Free flow area of the shell $A_{\text{free}} = \frac{\pi}{4}\left(D_i^2 - N_t \times d_0^2\right)$ (12)

Fluid free flow area of the tube $A_{t,\text{free}} = \frac{\pi}{4} d_i^2$ (13)

Shell side fluid velocity is $V_s = \frac{\dot{m}_s}{\rho_s A_s}$ (14)

Liter per minute (LPM) =14, 17, 20, 23 and 26.

Volume flow rate $\left(\frac{m^3}{s}\right) = \frac{\text{Liter per minute}}{60 \times 1000}$ (15)

Mass flow rate $m_s = \text{Volume flow rate} \times \text{Density of shell side fluid} \frac{\text{kg}}{s}$ (16)

Shell side free flow area $A_s(m^2) = \frac{\pi}{4}\left(D_i^2 - N_t d_0^2\right)$ (17)

$V_s\left(\frac{m}{s}\right) = \frac{m_s}{\rho_s A_s}$ (18)

Liter per minute (LPM) =13, 16,19, 22 and 25.

Volume flow rate $\left(\frac{m^3}{s}\right) = \frac{\text{Liter per minute}}{60 \times 1000}$ (19)

Mass flow rate m_t = Volume flow rate × Density of tube side fluid $\frac{\text{kg}}{s}$

(20)

The velocity of the fluid in the tubes is $V_t = \frac{N_p}{N_t}\frac{4\dot{m}_t}{\pi d_i^2 \rho_t}$

(21)

Where N_p is the number of tube passes and N_t is the total number of tubes

Tube side fluid velocity $V_t = \frac{n_p \times m_t}{N_t \times \frac{\pi}{4} \times d_i^2 \times \rho_t}$

(22)

Where, $n_p = 1$ for single pass fluid flow

The effectiveness of counter flow shell and tub heat exchanger depends on the heat capacity ratio and the number of heat transfer units (NTU) parameters given by Kakac and Liu

Heat exchanger effectiveness is

$$\varepsilon = \frac{1-e^{(-\text{NTU}(1-C))}}{1-\text{Ce}^{(-\text{NTU}(1-C))}}$$

(23)

Sometimes in literature heat exchanger effectiveness is termed as the thermal efficiency. It is non-dimensional, and it is depends on the number of transfer units (NTU), the heat capacity rate ratio

and the flow arrangement for direct transfer type heat exchanger.

Shell side

$C_{minimium}$ is the minimum of C_{hot} and C_{cold}

$$C^* = \frac{C_{\text{minimum}}}{C_{\text{maximum}}} = \frac{(\text{mC}_p)_{\text{minimum}}}{(\text{mC}_p)_{\text{maximum}}}$$

(24)

Heat exchanger surface Area is A_0 = N_t x πd_0 x L

(25)

Tube side flow cross section area per pass area is

$$A_0 = \frac{\pi}{4}\frac{d_i^2 N_t}{n_p}$$

(26)

Where, n_p=1 for single pass fluid flow

The number of transfer units

$$\text{NTU} = \frac{\text{UA}_0}{C_{\text{minimum}}} = \frac{\text{UA}_0}{(\text{mC}_p)_{\text{minimum}}}$$

(27)

Where U=1000 assumed,

The effectiveness of counter flow shell and tube heat exchangers depends on the heat capacity ratio C* and the number of heat transfer units (NTU) parameters given by Kakac and Liu as

$$\varepsilon = \frac{1-e^{(-\text{NTU}(1-c*))}}{1-c*e^{(-\text{NTU}(1-c*))}}$$

(28)

The outlet temperatures of both the fluids can be calculated by using the effectiveness and the inlet temperatures of both (hot and cold) the fluids.

Based on the C_{minimum} $\varepsilon = \frac{T_{t,o}-T_{t,i}}{T_{s,i}-T_{t,i}}$

(29)

$$T_{c,o} = T_{c,i} + \varepsilon(T_{h,i} - T_{c,i})$$

(30)

From the energy balance,

$$m_s C_{p,s}(T_{s,i} - T_{s,o}) = m_t C_{p,t}(T_{t,o} - T_{t,i})$$

$$(T_{s,i} - T_{s,o}) = \frac{m_t C_{p,t}}{m_s C_{p,s}}(T_{t,o} - T_{t,i})$$

$$T_{s,o} = T_{s,i} - \frac{m_t C_{p,t}}{m_s C_{p,s}}(T_{t,o} - T_{t,i})$$

(31)

Table 2: Outlet and bulk temperatures

$T_{s,i}$ in K	$T_{s,o}$ in K	$T_{s,b}$ in K	$T_{c,i}$ in K	$T_{c,o}$ in K	$T_{c,b}$ in K
343.15	333.54	338.69	301.15	313.07	305.95
	334.88	339.99		311.40	305.29
	335.92	340.80		310.12	304.77
	336.74	341.34		309.11	304.35
	337.40	341.71		308.29	304.02

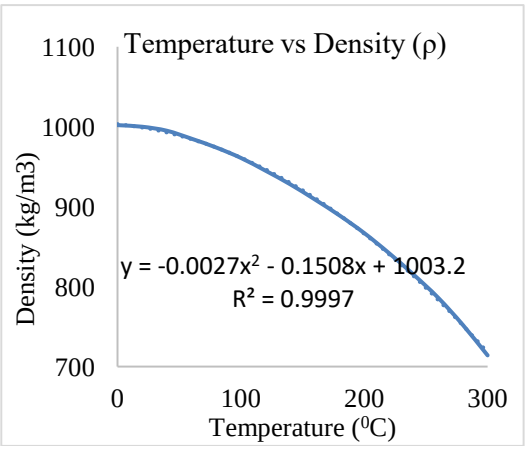

Fig. 1: Density Vs Temperature

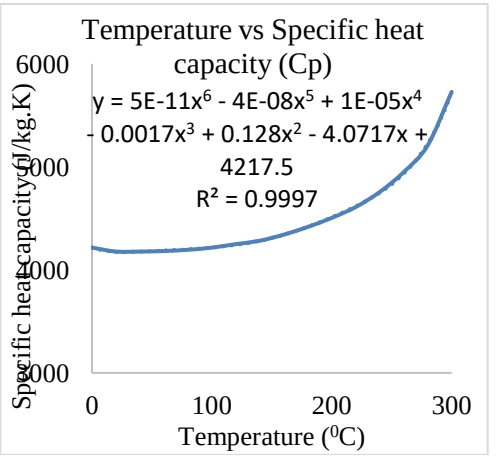

Fig. 2: Specific heat capacity Vs Temperature

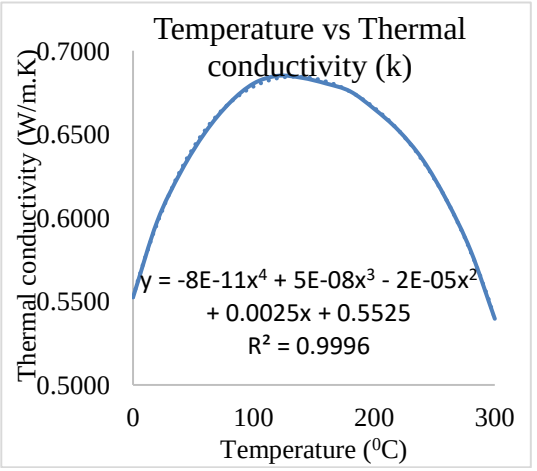

Fig. 3: Thermal conductivity Vs Temperature

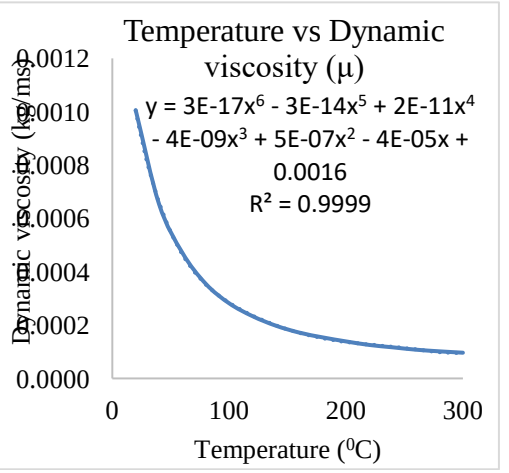

Fig. 4: Dynamic viscosity Vs Temperature

Table 3: Thermo-physical properties of water (H_2O)

Hot fluid (Shell side)	ρ_{hot}	981.7185	kg/m^3
	μ_{hot}	0.000335	m^2/s
	k_{hot}	0.6430	W/mK
	Cp_{hot}	4161.972	J/kgK
Cold fluid (Tube side)	ρ_{cold}	995.3482	kg/m^3
	μ_{cold}	0.000707	m^2/s
	k_{cold}	0.6147	W/mK
	Cp_{cold}	4171.785	J/kgK

The thermo-physical properties which are listed in table 3 are calculated based on the bulk fluid temperature. These thermos-physical properties are used to calculate the dimensionless numbers like Reynolds number, Prandtl number and Nusselt numbers.

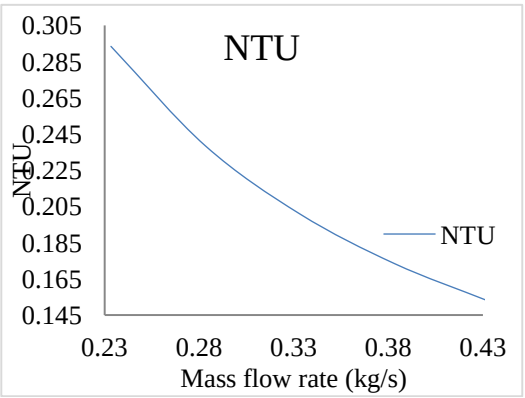

Fig. 5: NTU Vs Mass flow rate

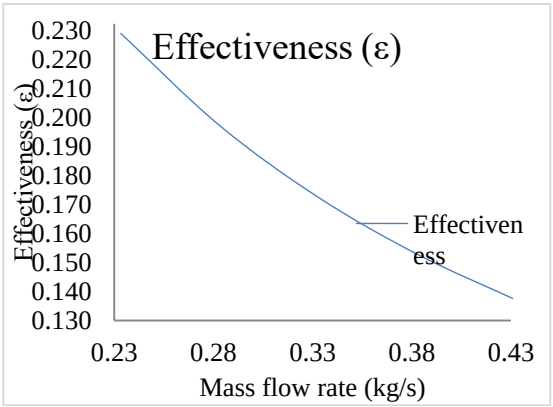

Fig. 6: Effectiveness Vs Mass flow rate

To plot above two figures, equation (27) and (28) are used to find NTU and effectiveness of shell and tube heat exchanger using counter flow. The effect of mass flow rate on NTU and effectiveness are shown in the fig. 5. The results indicate that effectiveness decreases with an increase in mass flow rate. In this study, mass flow rate through the tube and shell side both are varying. The decrease in effectiveness is due to the formation of a dead zone, which reduces the heat transfer rate. This study shows better agreement with Ram Kunwer et al.

Density

$$\rho = 0.002T^2 - 0.150T + 1003.2 \quad (32)$$

Specific Heat

$$C_p = 0.00000000005T^6 - 0.00000004T^5 + 0.00001T^4 - 0.001T^3 + 0.128T^2 - 4.071T4217 \quad (33)$$

Thermal conductivity

$$k = 0.000000000008T^4 + 0.00000005T^3 - 0.00002T^2 + 0.002T + 0.552 \quad (34)$$

Dynamic viscosity

$$\mu = 0.000000000000003T^5 + 0.00000000002T^4 - 0.000000004T^3 + 0.0000005T^2 - 0.00004T + 0.001 \quad (35)$$

Tube side heat transfer coefficient is calculated by Dittus-Boelter formula $h_t = 0.023\left(\frac{\lambda_t}{d_i}\right)\mathrm{Re}_t^{0.8}\mathrm{Pr}_t^{0.3}$

$$h_t = 0.023 \times \left(\frac{k_t}{d_i}\right) \times \mathrm{Re}_t^{0.8} \times \mathrm{Pr}_t^{0.4} \quad (36)$$

OR

Tube side Prandtl number is

$$\mathrm{Pr}_t = \frac{\mu_t C_{p_t}}{k_t}$$

(37)

Tube side Reynolds number

$$\mathrm{Re}_t = \frac{\rho_t v_t d_i}{\mu_t}$$

(38)

Tube side heat transfer coefficient $h_t = \frac{k_t}{d_i}\left[3.657 + \left(\frac{0.0677\left(\mathrm{Re}_t \mathrm{Pr}_t \frac{d_i}{L}\right)^{1.33}}{1+0.1\mathrm{Pr}_t\left(\mathrm{Re}_t \frac{d_i}{L}\right)^{0.3}}\right)\right]$ for $\mathrm{Re}_t < 2300$

(39)

$$h_t = \frac{k_t}{d_i}\left[\frac{\frac{f_t}{8}(\mathrm{Re}_t - 1000)\mathrm{Pr}_t}{1+12.7\sqrt{\frac{f_t}{8}}\left(\mathrm{Pr}_t^{\frac{2}{3}}-1\right)}\left[1+\left(\frac{d_i}{L}\right)^{0.67}\right]\right] \quad \text{for} \quad 2300 < \mathrm{Re}_t < 10{,}000$$

(40)

$$h_t = 0.027\frac{k_t}{d_i}\mathrm{Re}_t^{0.8}\mathrm{Pr}_t^{0.33}\left(\frac{\mu_t}{\mu_w}\right)^{0.14} \text{ for } \mathrm{Re}_t > 10{,}000$$

$$h_t = 0.023 \times \left(\frac{k_t}{d_i}\right) \times \mathrm{Re}_t^{0.8} \times \mathrm{Pr}_t^{0.4}$$

(41)

Shell side heat transfer rate $h_s = \frac{1}{\frac{1}{Q_{\text{avg}}} - \left(\frac{1}{h_t}\frac{d_0}{d_i}\right) - \left(\frac{d_0}{2k_t}\ln\left(\frac{d_0}{d_i}\right)\right)}$

(42)

$$Q_s = m_s \times c_{p,s} \times \left(T_{s,\text{in}} - T_{s,\text{out}}\right)$$

(43)

Tube side heat transfer rate $Q_t = M_t \times c_{p,t} \times \left(T_{t,\text{out}} - T_{t,\text{in}}\right)$

(44)

Average heat transfer rate

$$Q_{\text{ave}} = \frac{(Q_s + Q_t)}{2}$$

(45)

$$h_s = 0.023 \times \left(\frac{k_s}{D_e}\right) \times \mathrm{Re}_s^{0.8} \times \mathrm{Pr}_s^{0.3}$$

(46)

$$h_s = \frac{1}{\frac{1}{K} - \left(\frac{1}{h_t}\frac{d_0}{d_i}\right) - \left(\frac{d_0}{2k_w}\ln\left(\frac{d_0}{d_i}\right)\right)}$$

Shell side heat transfer coefficient

$$\frac{1}{U} = \frac{1}{h_t} \times \frac{d_0}{d_i} + \frac{d_0}{2\lambda_w} \ln\left(\frac{d_0}{d_i}\right) + \frac{1}{h_s}$$

(47)

% Difference$\frac{U_0 - U}{U} \times 100\%$

(48)

According to Kern's limitations, this difference may accept up to 30%.

Shell side Reynolds number $\mathrm{Re}_s = \frac{\rho_s v_s D_e}{\mu_s}$

(49)

$$\mathrm{Re}_s = \frac{m_s D_e}{A_{\mathrm{cross}} \mu_s}$$

Shell side Reynolds number is

(50)

$$A_{\mathrm{cross}} = B\left[(D_i - D_{\mathrm{otl}}) + \left(\frac{D_{\mathrm{otl}} - d_0}{P_t}\right)(P_t - d_0)\right]$$

For segmental baffle

(51)

For 75.5 mm baffle space

For non continuous helical baffles, the helical pitch is $B = \sqrt{2} D_s \tan(\beta_s)$

For continuous helical baffle, the helical pitch is $B = \pi D_s \tan(\beta_s)$

(52)

Shell side Reynolds number $\mathrm{Re}_s = \frac{\mathrm{ud}_0}{\nu_s}$

(53)

Where, $u = \frac{\mathrm{Volumeflowrate}}{\mathrm{CrossFlowArea}}$

The shell side Prandtl number is $\mathrm{Pr}_s = \frac{C_{\mathrm{ps}} \mu_s}{k_s}$

(54)

The overall heat transfer coefficient $K = \frac{Q_{\mathrm{ave}}}{A_0 \times \Delta T_m}$

(55)

Maximum temperature $\Delta T_{\max} = T_{s,\mathrm{in}} - T_{t,\mathrm{out}}$

Maximum temperature difference $\Delta T_{\max} = T_w - T_{\mathrm{in}}$

Minimum temperature difference $\Delta T_{\min} = T_{s,\mathrm{out}} - T_{t,\mathrm{in}}$

(56)

Minimum temperature difference $\Delta T_{\min} = T_w - T_{\text{out}}$ (57)

$$\Delta T_m = \left[\frac{\Delta T_{\max} - \Delta T_{\min}}{\ln\left(\frac{\Delta T_{\max}}{\Delta T_{\min}}\right)}\right]$$ (58)

$$K = \frac{Q_{\text{ave}}}{A_0 \times \Delta T_m}$$ (59)

Maximum temperature difference $\Delta T_{\max} = T_{s,\text{in}} - T_w$

Minimum temperature difference $\Delta T_{\min} = T_{s,\text{out}} - T_w$

Where T_w is the temperature of tube walls

$$\Delta T_m = \psi \left[\frac{\Delta T_{\max} - \Delta T_{\min}}{\ln\left(\frac{\Delta T_{\max}}{\Delta T_{\min}}\right)}\right]$$

$$\psi = \frac{\left(\sqrt{R^2+1}\right)\times\ln\left(\frac{1-P}{1-(P\times R)}\right)}{(R-1)\times\ln\left(\frac{2-P\left(R+1-\sqrt{R^2+1}\right)}{2-P\left(R+1+\sqrt{R^2+1}\right)}\right)}$$ for even number of tube passes

Ψ=1 for single pass

Efficiency $P = \frac{T_{t,\text{out}} - T_{t,\text{in}}}{T_{s,\text{in}} - T_{t,\text{in}}}$

Correction coefficient $R = \frac{T_{s,\text{in}} - T_{s,\text{out}}}{T_{t,\text{out}} - T_{t,\text{in}}}$

Tube side heat transfer coefficient is calculated using Gnielinski equation

$$\text{Nu}_t = \frac{\left(\frac{f_t}{8}\right)(\text{Re} - 1000) \times \text{Pr}_t}{1 + 12.7\left(\sqrt{\frac{f_t}{8}}\right)\left(\text{Pr}_t^{\frac{2}{3}} - 1\right)} \times \left[1 + \left(\frac{d_i}{L}\right)^{\frac{2}{3}}\right] \times c_t$$

$$c_t = \left(\frac{\text{Pr}_f}{\text{Pr}_w}\right)^{0.11}$$

The Colebrook's equation $f_t = \frac{1}{(0.782\times\ln(\text{Re}_t) - 1.51)^2}$ (60)

The Petukhov's correlation is $f_t = \frac{1}{(1.82\times\text{Re}_t - 1.64)^2}$ (61)

The Darcy friction factor/The Colebrook's equation is $f_t = \frac{1}{(1.82\ln(\mathrm{Re}_t)-1.64)^2}$ (62)

Friction factors is calculated by using Hagen-Poiseuille equation is

for laminar flow is ft=64/Re Re<=2*10^5 (63)

Friction factor for turbulent flow is ft=0.079/Re$^{0.25}$ Re<=2*10^5 (64)

Heat transfer coefficient

$$h_t = 0.023\left(\frac{k_t}{d_i}\right)\mathrm{Re}_t^{0.8}\mathrm{Pr}_t^{\frac{1}{3}}\left(\frac{\mu_t}{\mu_{\mathrm{tw}}}\right)^{0.14}$$

According to Kern's shell side heat transfer coefficient for segmental baffled shell and tube exchangers

$$h_s = 0.36\frac{\lambda}{D_e}\mathrm{Re}_s^{0.55}\mathrm{Pr}_s^{\frac{1}{3}}\left(\frac{\mu_t}{\mu_w}\right)^{0.14}$$

$$\mathrm{Nu}_s = c \times \mathrm{Re}_s^m \times \mathrm{Pr}_s^{\frac{1}{3}}$$

Shell side Nusselt number is $\mathrm{Nu}_s = \frac{h_s d_0}{\lambda_s}$ (65)

Sielder Tate $\mathrm{Nu} = 1.86\left(\mathrm{RePr}\frac{D}{L}\right)^{\frac{1}{3}}$ for laminar flow

$$f_s = c_2\mathrm{Re}_s^{m_1}$$

For Segmental baffle $\mathrm{Nu}_s = 0.012\mathrm{Re}_s^{0.98} \times \mathrm{Pr}_s^{\frac{1}{3}}$

For helical baffle $\mathrm{Nu}_s = 0.037\mathrm{Re}_s^{0.75} \times \mathrm{Pr}_s^{\frac{1}{3}}$

The shell side pressure drop is

$$\Delta P_s = \frac{\rho_s v_s^2}{2} f_s \frac{L}{B}\frac{D_s}{D_e}$$

Where Ps is shell side pressure drop

ρ_s shell side fluid density

L is the length of the tube in mm

Shell side friction factor $f_s = \frac{2b_0}{\mathrm{Re}_s^{0.15}}$

From Peters and Timmer Haus

$$b_0 = 0.72 \text{ where } \mathrm{Re}_s < 40{,}000$$

Swirl angle of fluid flow in helical channel $\beta^0 = \arctan\left(\frac{V_P}{V_R}\right)$

Where, $V_P = V_a$

$V_R = \sqrt{V_t^2 + V_r^2}$

Va, Vt and Vr are the axial, tangential and radial components of velocity.

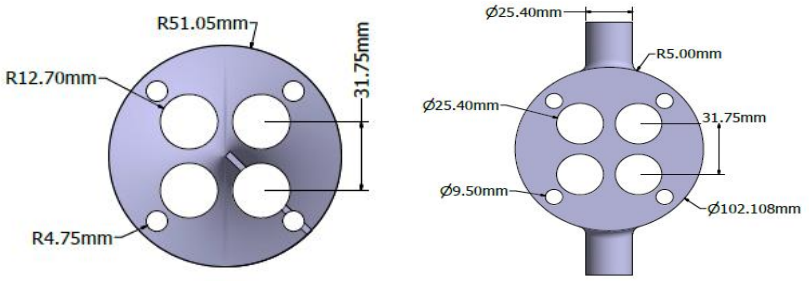

Fig. 7: Side view of shell and tube heat exchanger

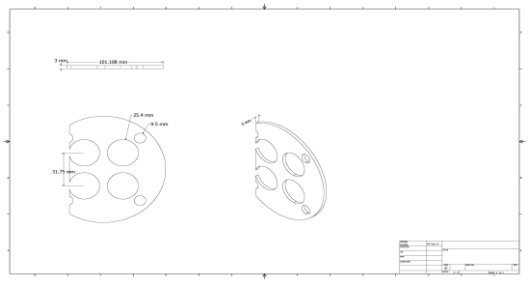

Figure 8: 22% cut segmental baffles for shell and tube exchanger

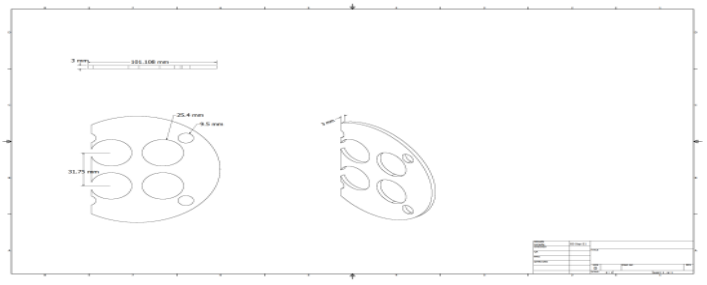

Figure 9: Front and side view of shell and tube heat exchanger

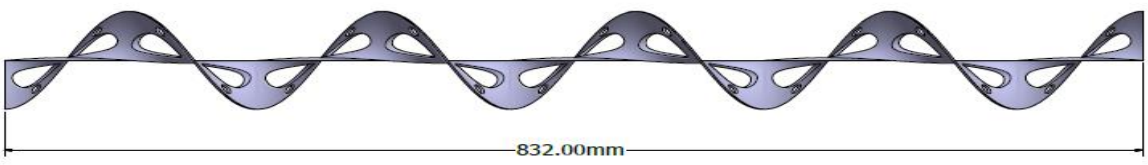

Fig. 10: Front view of helical baffles for shell and tube heat exchanger

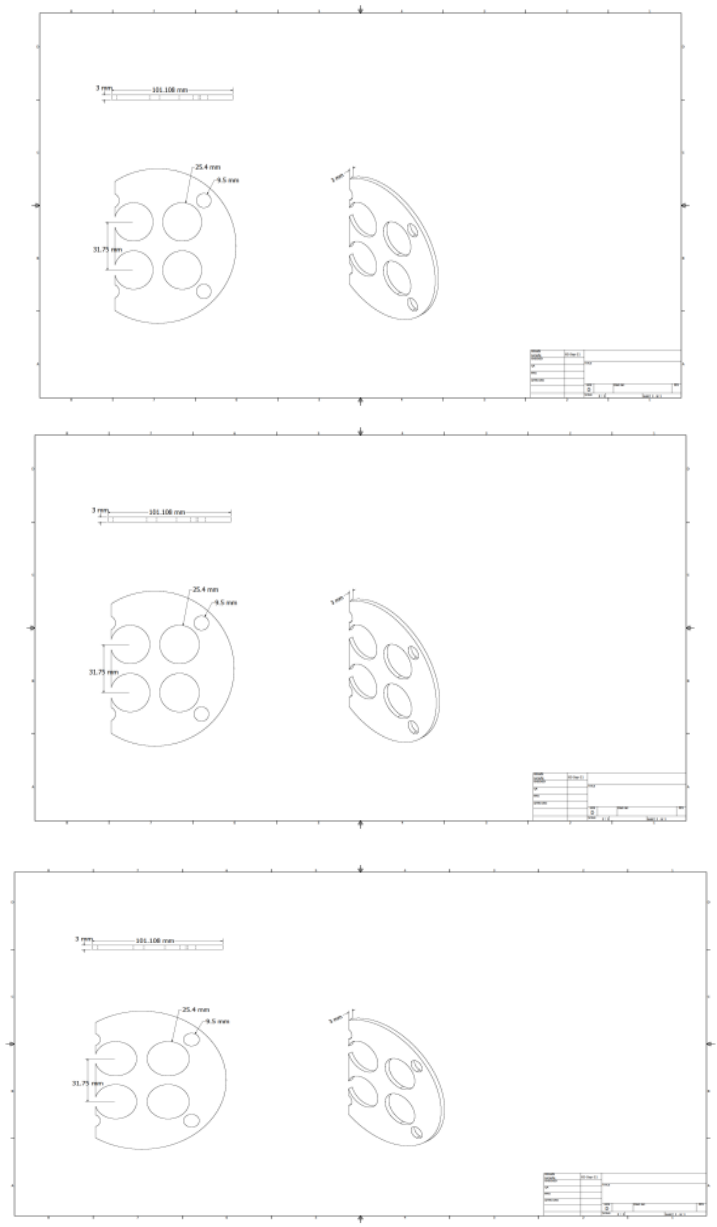

Fig. 11: Front view of helical baffles (20^0, 30^0, 40^0) for shell and tube heat exchanger

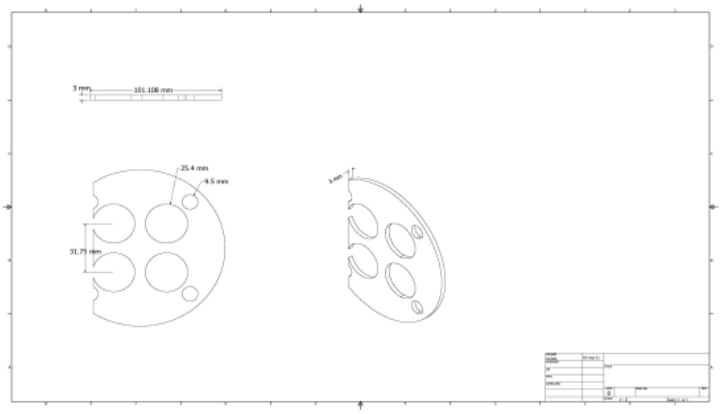

Fig. 12: Tubes for shell and tube heat exchangers

Governing equations and boundary conditions

The renormalization group (RNG) $k-\varepsilon$ model is adopted in the simulation because the model provides improved predictions of near-wall flows. The RNG $k-\varepsilon$model was derived by a statistical technique called renormalization method, which is widely used in industrial flow and heat transfer because of its economy and accuracy. The governing equations for continuity, momentum, energy, k and ε in the computational domain can be expressed as follows:

Continuity equation: $\frac{\partial(\rho u_i)}{\partial x_i}=0$

Momentum equation: $\frac{\partial(\rho u_i u_k)}{\partial x_i}+\frac{\partial P}{\partial x_k}-\frac{\partial\left(\mu\frac{\partial u_k}{\partial x_i}\right)}{\partial x_i}=0$

Energy equation: $\frac{\partial(\rho u_i t)}{\partial x_i}-\frac{\partial\left(\frac{k}{C_p}\times\frac{\partial t}{\partial x_i}\right)}{\partial x_i}=0$

Turbulent kinetic energy equation: $\frac{\partial(\rho k)}{\partial t}-\frac{\partial\left(\alpha_k\mu_{\text{eff}}\frac{\partial k}{\partial x_j}\right)}{\partial x_j}+\frac{\partial(\rho \text{ku}_i)}{\partial x_i}+\rho\varepsilon-G_k=0$

Turbulent dissipation energy equation: $\frac{\partial(\rho\varepsilon)}{\partial t}-\frac{\partial\left(\alpha_\varepsilon\mu_{\text{eff}}\frac{\partial \varepsilon}{\partial x_j}\right)}{\partial x_j}+\frac{\partial(\rho u_i\varepsilon)}{\partial x_i}-C_{1\varepsilon}^{*}\frac{\varepsilon G_k}{k}+\frac{\rho C_{2\varepsilon}\varepsilon^2}{k}=0$

Where,

$\mu_{\text{eff}}=\mu+\frac{\rho c_\mu k^2}{\varepsilon}$

$C_{1\varepsilon}^{*}=C_{1\varepsilon}-\frac{\eta\left(1-\frac{\eta}{\eta_0}\right)}{1+\eta^3\beta}$

$$\eta = \frac{k\sqrt{2E_{ij}.E_{ij}}}{\varepsilon}$$

$$E_{ij} = 0.5\left[\frac{\partial u_i}{\partial x_j} + \frac{\partial u_j}{\partial x_i}\right]$$

The empirical constants for the RNG k − εmodel are assigned the following value:

$C_\mu = 84.5 \times 10^{-3}$

$C_{1\varepsilon} = 142 \times 10^{-2}$

$C_{2\varepsilon} = 168 \times 10^{-2}$

$\beta = 12 \times 10^{-3}$

$\eta_0 = 438 \times 10^{-2}$

$\alpha_k = \alpha_\varepsilon = 139 \times 10^{-2}$

Non-slip boundary condition is adopted on the wall. The standard wall function method is used. The wall temperatures of the tubes and shell are uniform and fixed to 301.15 K and 343.15 K respectively. The internal surfaces of the shell are non-slip, impermeable and adiabatic. Hot fluid is adopted as shell side and cold fluid is adopted as tube side working fluid. The boundary conditions of shell side inlet and outlet are mass flow rate (kg/s) and atmospheric pressure as outlet.

Mesh Generation and Boundary Conditions

A tetrahedral unstructured mesh was chosen for the 3D geometry in ANSYS to optimize complex fluid flow simulations, using the RNG k-ε model for accurate wall treatment.

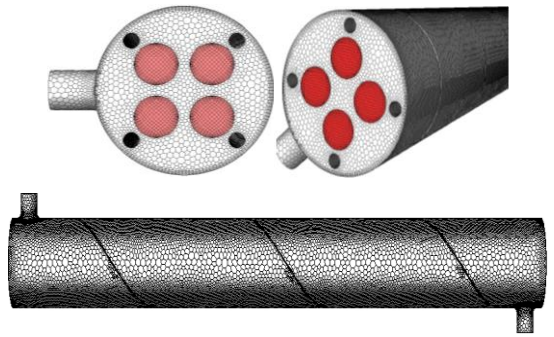

Fig. 13: Selection view of generated Mesh

Hot (shell) and cold (tube) water with specified thermo-physical properties (Table 3) are simulated in a counter-flow setup in the STHX, with a coupled thermal boundary, no-slip walls, and adiabatic outlets for incompressible, viscous 3D flow at constant temperatures of 343.15 K and 301.15 K.

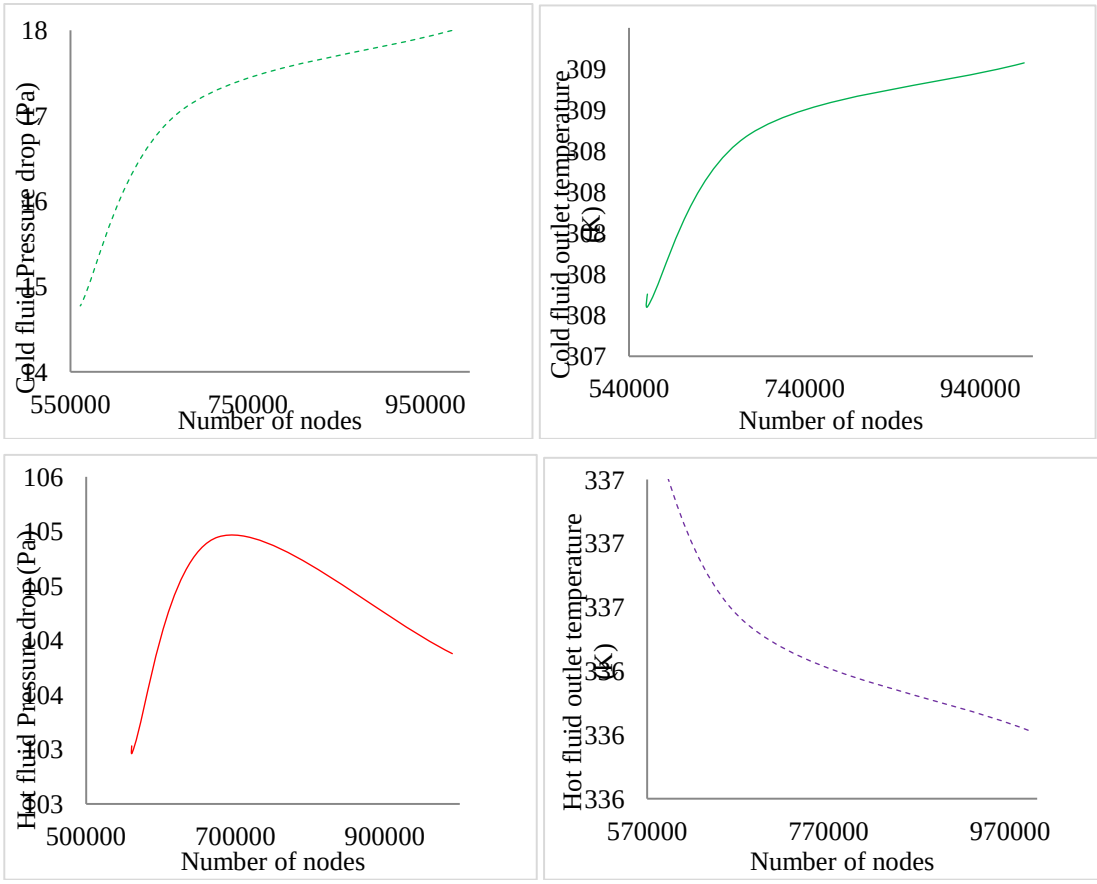

Fig. 14: Validation test

A grid of 9.90022 million nodes and 0.002 m element size was selected for optimized accuracy, achieving stable outlet temperatures, pressure drop, and grid independence, with an average orthogonal quality of 0.82, skewness of 0.2, and aspect ratio of 2.6.

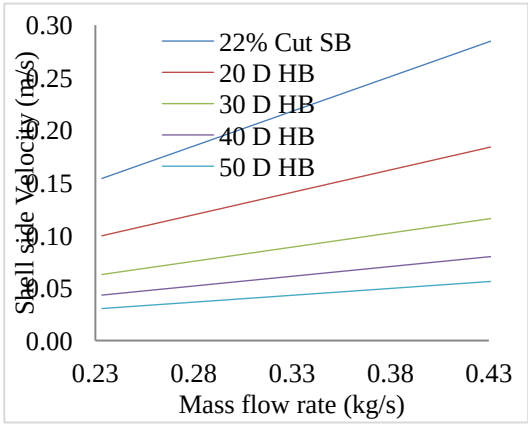

Fig. 15: Shell side velocity

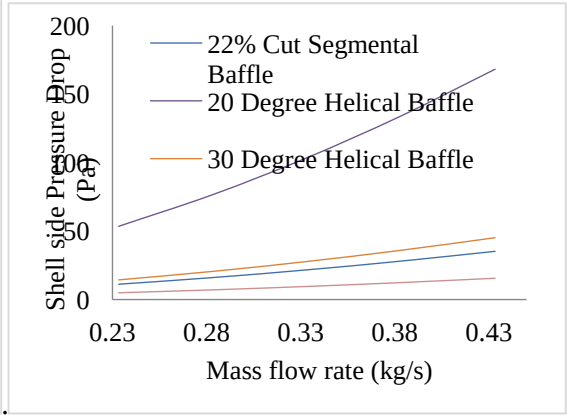

Fig. 16: Shell side pressure drop

Larger helical angles result in lower shell-side velocities and reduced pressure drops, with the 22% cut segmental baffle showing the highest velocity and the 40^0 helical baffle achieving the lowest pressure drop, consistent with prior studies.

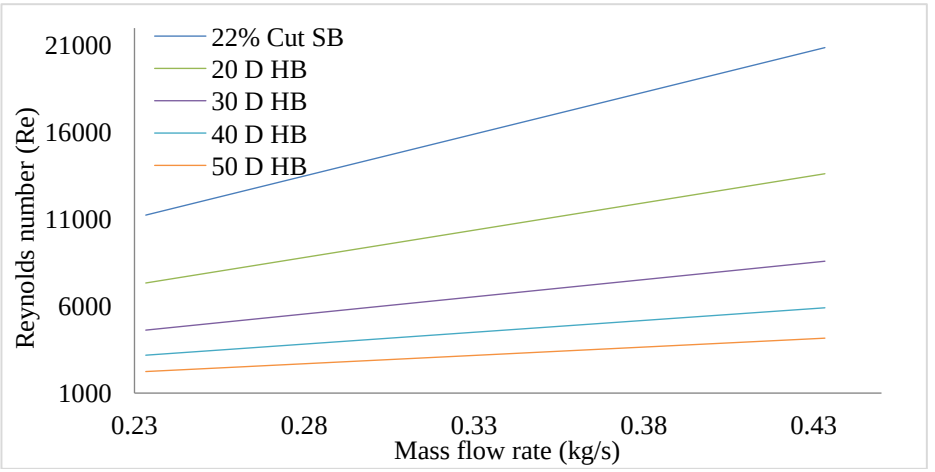

Figure 17: Shell side Reynolds number

Reynolds number increases with mass flow rate for all heat exchangers, with helical baffles showing higher increases compared to the 22% cut segmental baffle, reaching 80.08% for the 50^0 helical baffle.

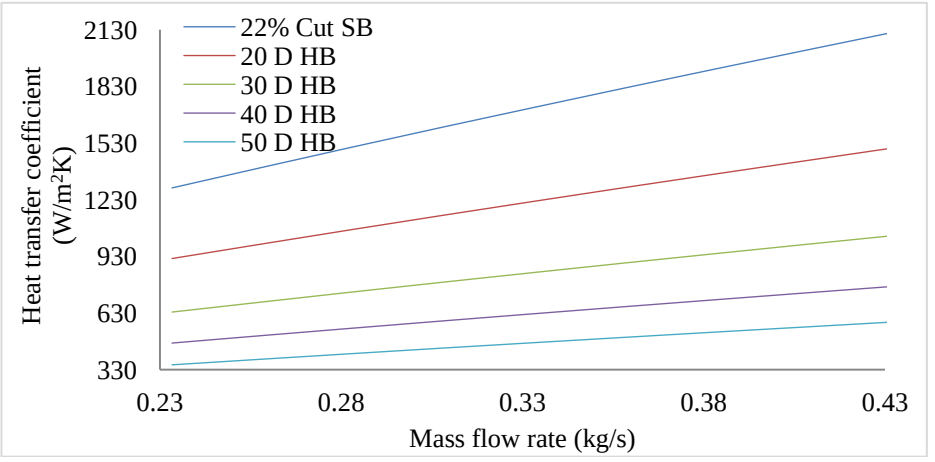

Figure 18: Shell side heat transfer coefficient

The heat transfer coefficient increases with mass flow rate, with the 22% cut segmental baffle achieving the highest values, while helical baffles show lower coefficients that decrease as the helix angle increases, consistent with previous findings.

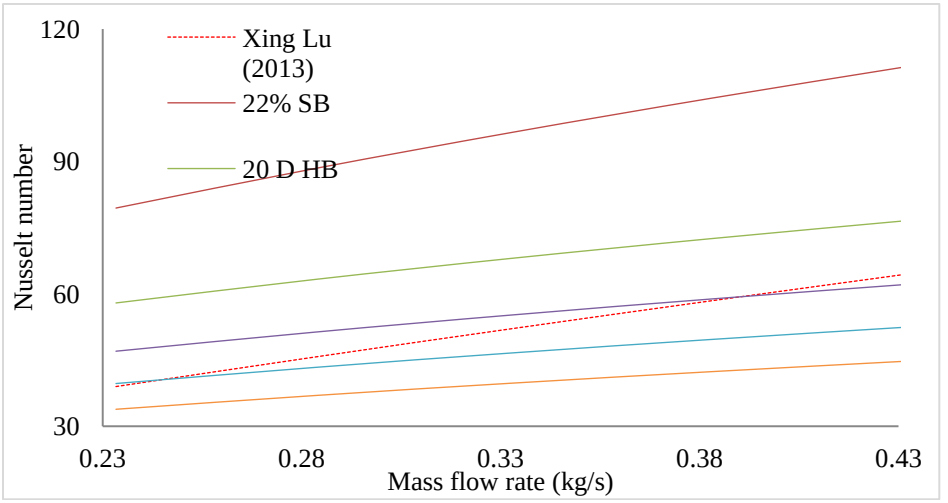

Figure 19: Shell side Nusselt number

Nusselt number increases with mass flow rate, showing a 1.73% difference compared to Xing Lu's model for the 40^0 helical baffle; however, it decreases with larger helical angles at the same mass flow rate, consistent with Simin Wang's findings.

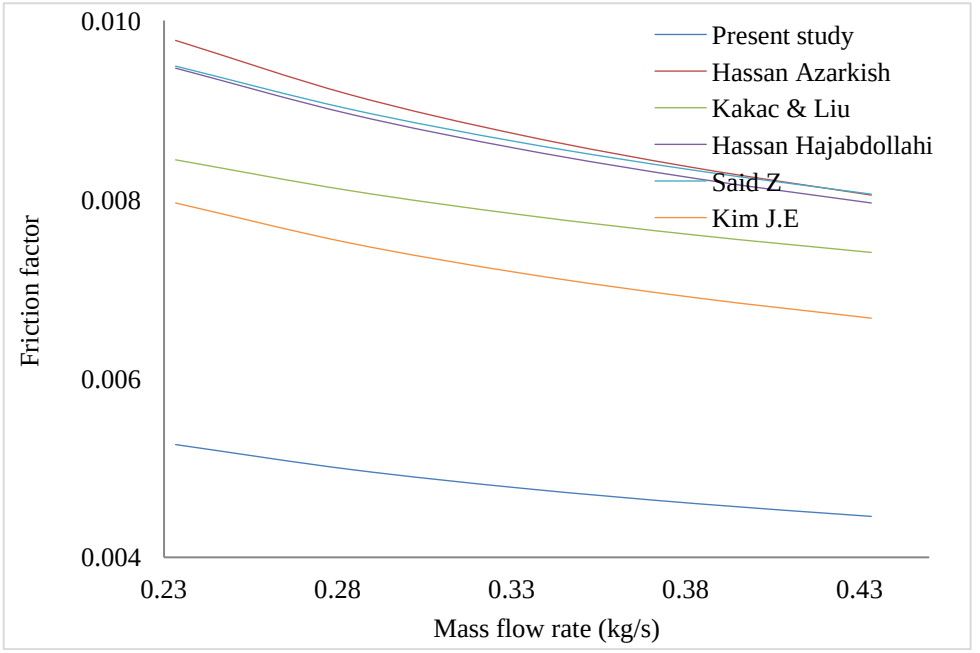

Figure 20: Friction factor in tube

Friction factor decreases with the increase of mass flow rate. The friction factor is calculated by using equation (60) to (62). In figure 20 all the empirical equations/relations are calculated and were compared, all are having good agreement and following same trends. Among the studied friction factor equations/relations, present work has less friction factor.

3. Conclusions:

The study investigates shell and tube heat exchangers, revealing that effectiveness decreases with increasing mass flow rate due to dead zones that reduce heat transfer, as noted by Ram Kunwer et al. Shell side velocity decreases with larger helical angles; 22% cut segmental baffles have the highest velocity, while 50° helical baffles have the lowest, aligning with findings from Simin Wang et al.

Pressure drop is lower with higher helical angles, with the 40° helical baffle showing the least drop. Reynolds numbers increase with mass flow rate, with reductions of 34.75% to 80.08% for helical baffles compared to the 22% cut segmental baffle. Heat transfer coefficients also increase with mass flow rate, with the segmental baffle outperforming helical designs by significant margins.

The Nusselt number rises with mass flow rate, with only a 1.73% deviation from Xing Lu's model for the 40° helical baffle. Friction factors decrease with mass flow rate, with the present study showing lower values compared to existing empirical models, indicating strong agreement across analyzed equations.

References

1. Arjun kumar prasad Design & Analysis of Shell & Tube Type Heat Exchanger, International Journal of Engineering Research & Technology (IJERT)Vol. 9 Issue 01, January-2020 ISSN: 2278-0181.
2. Roetzel W and Lee D. Experimental investigation of leakage in shell and tube heat exchangers with segmental baffles. International Journal of Heat Mass Transfer 1993; 36: pp: 3765-3771.
3. Waseem Al Hadad, Vincent Schick and Denis Maillet. Fouling detection in a shell and tube heat exchanger using variation of its thermal impulse responses: Methodological approach and numerical verification. Applied Thermal Engineering 2019; Vol.: 155, pp: 612-619.
4. Huadong Li and Volker Kottke. Effect of the leakage on pressure drop and local heat transfer in shell and tube heat exchangers for staggered tube arrangement. International Journal of Heat Mass Transfer, 1998, Vol.: 41, No.: 2, pp: 425-433.
5. Wilfried Roetzel and Deiying W Lee. Effect of baffle/shell leakage flow on heat transfer in shell and tube heat exchangers. Experimental Thermal and Fluid Science, 1994; Vol.: 8, pp: 10-20.
6. Halle H, Chenoweth J.M and Wambsganss. Flow induced vibration in shell and tube heat exchangers with double segmental baffles. Heat Transfer Engineering, 1986; Vol.: 7, No.: 3-4, pp: 64-71.
7. Halle H, Chenoweth J.M and Wambsganss W.M. Shell side water flow pressure drop distribution measurements in an industrial sized test heat exchanger. Transactions of the ASME, 1988; Vol.: 110, pp: 60-67.
8. Mustapha Mellal, Redouane Benzeguir, Djamel Sahel and Houari Ameur. Hydro-thermal shell side performance evaluation of a shell and tube heat exchanger under different baffle arrangement and orientation. International Journal of Thermal Sciences, 2017; Vol.: 121, pp: 138-149.
9. Anuruddha Bhattacharjee, Asif Ahmed and Sumon Saha. Influence of helix angle on the performance of shell and tube heat exchanger with continuous helical baffle. International conference on mechanical engineering, 2017, 20th-22nd December, Dhaka, Bangladesh.

10. Asif Ahmed, Imam UI Ferdous and Sumon Saha. Comparison of performance of shell and tube heat exchangers with conventional segmental baffles and continuous helical baffle. 7th BSME International Conference on Thermal Engineering, AIP conference proceeding, 1851, 020066: 1-12.
11. Bashir I Master, Krishnan S. Chunangad ans Venkateswaran Pushpanathan. Fouling Mitigation using Helixchanger Heat Exchangers. Published by ECI DigitalnArchives, 2003,pp:1-6
12. Bashir I Master, Chunangad K.S, Boxma A.J, Kral D and Stehlik P. Most frequently used heat exchangers from pioneering research to worldwide applications. Heat Transfer Engineering, 2006; Vol.: 27, No.: 6, pp: 4-11.
13. Cong Dong, Ya Ping Chen and Jia Feng Wu. Influence of baffle configurations on flow and heat transfer characteristic of trisection helical baffle heat exchangers. Energy Conversion and Management, 2014; Vol.: 88, pp: 251-258.
14. Cong Dong, Yaping Chen and Jiafeng Wu. Comparison of heat transfer performances of helix baffled heat exchangers with different baffle configurations. Chinese Journal of Chemical Engineering, 2015; Vol.: 23, pp: 255-261.
15. Cong Don, Dongshuang Li, Youqu Zheng, Guoneng Li, Yange Suo and Yaping Chen. An efficient and low resistant circumferential overlap trisection helical baffle heat exchanger with folded baffles. Energy Conversion and Management, 2016; Vol.: 113, pp: 143-152.
16. Farhad Nemati Taher, Sirous Zeyninejad Movassag, Kazem Razmi and Reza Tasouji Azar. Baffle space impact on the performance of helical baffle shell and tube heat exchangers. Applied Thermal Engineering, 2012, Vol.: 44, pp: 143-149.
17. Jian Chen, Xing Lu, Qiuwang Wang and Min Zeng. Experimental investigation on thermal hydraulic performance of a novel shell and tube heat exchanger with unilateral ladder type helical baffles. Applied Thermal Engineering, 161, 2019, 114099.
18. Jian Fei Zhang, Shao Long Guo, Zhong Zhen Li, Jin Ping Wang, Ya Ling He and Wen Quan Tao. Experimental performance comparison of shell and tube oil coolers with overlapped helical baffles and segmental baffles. Applied Thermal Engineering, 2013; Vol.: 58, pp: 336-343.
19. Jian Fei Zhang, Bin Li, Wen Jiang Huang, Yong Gang Lei, Ya Ling He and Wen Quan Tao. Experimental performance comparison of shell side heat transfer for shell and tube heat exchangers with middle overlapped helical baffles and segmental baffles. Chemical Engineering Science, 2009; Vol.: 64, pp: 1643-1653.
20. Jian Wen, Huizhu Yang, Simin Wang, YulanXue and Xin Tong. Experimental investigation on performance comparison for shell and tube heat exchangers with different baffles. International Journal of Heat and Mass Transfer, 2015; Vol.: 84, pp: 990-997.
21. Jian Wen, Huizhu Yang, Simin Wang, Shifeng Xu, YulanXue and HanfeiTuo. Numerical investigation on baffle configuration improvement of the heat exchanger with helical baffles. Energy Conversion and Management, 2015; Vol.: 89, pp: 438-448.
22. Juan Xiao, Simin Wang, Shupei Ye, Jiarui Wang, Jian Wen and Jiyuan Tu. Experimental investigation on pre heating technology of coal water slurry with different concentration in shell and tube heat exchangers with ladder type fold baffles. International Journal of Heat and Mass Transfer, 2019; Vol.: 132, pp: 1116-1125.
23. Kral D, Stehlik P, Van Der Ploeg H.J and Bashir I Master. Helical Baffles in shell and tube heat exchangers, Part I: Experimental Verification, Heat Transfer Engineering, 1996; Vol.: 17:1, pp: 93-101.
24. Malcolm J Andrews and Bashir I Master. Three Dimensional Modeling of a Helixchanger Heat Exchanger Using CFD. Heat Transfer Engineering, 2005; 26(6), pp: 22-31.
25. Manasa Kishtapati and Meda Kalyan Kumar. Improvisation of Shell Side Heat Transfer Coefficient in Shell and Tube Heat Exchangers using Different Configurations-A Mini Review.

International Journal of Engineering Research & Technology (IJERT) 2015; 04 (06), pp: 1125-1130.
26. Peng B, Wang Q.W, Zhang C, Xie G.N, Luo L.Q, Chen Q.Y and Zeng M. An experimental study of shell and tube heat exchangers with continuous helical baffles. Journal of heat transfer, 2007; Vol.: 129, pp: 1425-1431.
27. Ram Kunwer, Shyam Pandey, Swapnil Sureshchandra Bhurat (2020). Comparison of selected shell and tube heat exchangers with segmental and helical baffles, Thermal Science and Engineering Progress, 20, 2020, 100712.
28. Simin Wang, Jian Wen, Huizhu Yang, Yulan Xue and Hanfei Tuo. Experimental investigation on heat transfer enhancement of a heat exchanger with helical baffles through blockage of triangle leakage zones. Applied Thermal Engineering, 2014; Vol.: 67, pp: 122-130.
29. Simin Wang, Juan Xiao, Shupei Ye, Chen Song and Jian Wen. Numerical investigation on pre-heating of coal water slurry in shell and tube heat exchangers with fold helical baffles. International Journal of Heat and Mass Transfer, 2018; Vol.: 126, pp: 1347-1355.
30. Stehlik P, Nemcansky J, Kral D and Swanson L.W. Comparison of correction factors for shell and tube heat exchangers with segmental or helical baffles. Heat transfer engineering, 1994; Vol.: 15, No.: 1, pp: 55-65.
31. Sunil Shinde and Umesh Chavan. Numerical and experimental analysis on shell side thermo-hydraulic performance of shell and tube heat exchanger with continuous helical FRP baffles. Thermal Science and Engineering Progress, 2018, Vol.: 5, pp: 158-171.
32. Usman Salahuddin, Muhammad Bilal and Haider Ejaz. A review of the advancements made in helical baffles used in shell and tube heat exchangers. International Communications in Heat and Mass Transfer, 2015; Vol.: 67, pp: 104-108.
33. Wang Wei han, Cheng Dao lai, Liu Tao and Liu Ying hao. Performance comparison for oil-water heat transfer of circumferential overlap trisection helical baffle heat exchanger. Journal of South Central University, 2016; Vol.: 23, pp: 2720-2727.
34. Wenjing DU, Wang Hongfu and Cheng Lin. Effects of shape and quantity of helical baffle on the shell side heat transfer and flow performance of heat exchangers. Fluid Dynamics and Transport Phenomena, Chiness Journal of Chemical Engineering, 2014; Vol.: 22(3), pp: 243-251.
35. Xiaoming Xiao, Luhong Zhang, Xingang Li, Bing Jiang, Xiaoling Yang and Youmei Xia. Numerical investigation of helical baffles heat exchanger with different Prandtl number fluids. International Journal of Heat and Mass Transfer, 2013; Vol.: 63, pp: 434-444.
36. Ya Ping Chen, Yan Jun Sheng, Cong Dong and Jia Feng Wu. Numerical simulation on flow field in circumferential overlap trisection helical baffle heat exchanger. Applied Thermal Engineering, 2013; Vol.: 50, pp: 1035-1043.
37. Ya Ping Chen, Wei han Wang, Jia Feng Wu and Cong Dong. Experimental investigation on performances of trisection helical baffled heat exchangers for oil/water-water heat transfer. Energy Conversion and Management 2015; 101: pp: 460-469.
38. Yong Gang Lei, Ya Ling He, Rui Li and Ya Fu Gao. Effects of baffle inclination angle on flow and heat transfer of a heat exchanger with helical baffles. Chemical Engineering and Processing, 2008, Vol.: 47, pp: 2336-2345.
39. Yong Gang Lei, Ya Ling He, Pan Chu and Rui Li. Design and optimization of heat exchangers with helical baffles. Chemical Engineering Science, 2008; Vol.: 63, pp: 4386-4395.
40. Zhengguo Zhang, Dabin Ma, Xiaoming Fang and Xuenong Gao. Experimental and numerical heat transfer in a helically baffled heat exchanger combined with one three dimensional finned tube. Chemical Engineering and Processing, 2008, Vol.: 47, pp: 1738-1743.